

Final Report for Phase 1  
Contract No. E-43-4

“Chemical Analysis of Diesel Nanoparticles Using a  
Nano-DMA/Thermal Desorption Particle Beam Mass Spectrometer”

September 1, 2000

Principal Investigator: Professor Paul J. Ziemann, Air Pollution Research Center, University of  
California, Riverside, CA 92521

Subcontractor: Peter H. McMurry, Particle Technology Laboratory, Department of Mechanical  
Engineering, University of Minnesota, Minneapolis, MN 55455

---

Paul J. Ziemann  
Principal Investigator  
Phone: (909) 787-5127  
FAX: (909) 787-5004  
Email: paul.ziemann@ucr.edu

## TABLE OF CONTENTS

	Page
1. Summary.....	2
2. Background.....	2
3. Objectives .....	4
4. Approach.....	6
5. Results.....	6
5.1. Project Personnel.....	6
5.2. Preliminary Research at UCR and UMN.....	6
5.2.1. Ziemann Group Experiments at UCR.....	6
5.2.2. McMurry Group Experiments at UMN.....	7
5.3. Diesel Nanoparticle Study at UMNCDR.....	7
5.3.1. Shipping, Set-up, and Preliminary Testing.....	8
5.3.2. Methods.....	9
5.3.2.1. Diesel Engine and Operation.....	9
5.3.2.2. Diesel Engine Exhaust Sampling.....	9
5.3.2.3. Particle Size Selection and Size Distribution Measurements.....	10
5.3.2.4. TDPBMS Particle Sampling and Fast-TPTD Analysis.....	11
5.3.2.5. Mass Spectral Analysis: Full Scan or Five-Mass SIM.....	12
5.3.2.6. TDPBMS Calibration and Standards Analysis.....	13
5.3.2.7. Materials.....	14
5.3.2.8. Electrostatic Focusing Experiments.....	14
5.3.3. Results.....	14
5.3.3.1. Experimental Matrix.....	14
5.3.3.2. Particle Mass Spectra.....	15
5.3.3.3. Effect of Engine Load and Particle Size on Composition and Volatility of Organic Aerosol.....	17
5.3.3.4. Evidence for Sulfuric Acid in Nanoparticles.....	18
5.3.3.5. Mechanism of Diesel Nanoparticle Formation.....	20
6. Conclusions.....	21
7. Future Plans.....	22
7.1. Phase 1.....	22
7.2. Phase 2.....	22
8. References.....	23
9. Figures and Tables.....	25

## 1. SUMMARY

This report describes the results of Phase 1 of our project, "Chemical Analysis of Diesel Nanoparticles Using a Nano-DMA/Thermal Desorption Particle Beam Mass Spectrometer", Contract No. E-43-4. The project involves a collaboration between the research groups of Professor Paul Ziemann at the University of California, Riverside (UCR) and Professor Peter McMurry at the University of Minnesota (UMN) and covers the period 2/7/2000-9/7/2001. Phase 1 work has included preliminary experiments at UCR and UMN, a one-month study of diesel nanoparticle chemistry carried out in collaboration with Professor David Kittelson and staff at the University of Minnesota Center for Diesel Research (UMNCDR), and subsequent data analysis and writing. The data analysis is essentially complete, and it can be stated without hesitation that the diesel study was a clear success. This is the first time that particles in the nanoparticle size mode have been cleanly sampled from a diesel engine and chemically analyzed, and a great deal of new information on nanoparticle composition was obtained. Using the Nano-DMA/thermal desorption particle beam mass spectrometer for near-real time analysis we were able to identify and determine average carbon numbers and vapor pressures for the major classes of organic components, which make up the bulk of the nanoparticle mass, for aerosol samples down to ~25 nm mass median diameter (MMD). The organic mass spectra are similar for all sizes of diesel particles, fuel, and lubricating oil, indicating that the source of particulate organics is unburned fuel and/or oil. The volatility of the organic fraction of the aerosol decreases as engine load increases and as particle size decreases. We were also able to detect low concentrations of sulfuric acid in particles as small as ~40 nm MMD. The results are consistent with a mechanism of diesel nanoparticle formation involving homogeneous binary nucleation of sulfuric acid and water followed by particle growth from condensation of successively more volatile organic species onto the sulfuric acid-water core.

## 2. BACKGROUND

Recent epidemiological studies have found an association between atmospheric fine particle (diameter < 2.5  $\mu\text{m}$ ) mass concentrations, and exacerbation of illness in people with respiratory disease and increased mortality among older people with respiratory and cardiovascular disease (1, 2). These studies have led the U.S. Environmental Protection Agency to propose a new fine particle standard, which is somewhat controversial and has not yet been implemented because of legal challenges. Unlike air quality standards for gaseous compounds such as ozone or carbon monoxide, the particle standard is based on particulate mass without regard to chemical composition. Because of the complex nature of atmospheric particulate matter, developing a possible mechanism for health effects will require more detailed knowledge of the size-dependent chemical composition of fine particles.

One important source of fine particles is combustion, which occurs both naturally and through human activities. Modern combustion engines burn cleaner and produce less particulate mass than older models, but it has also been observed that some engines, for example diesels, emit high concentrations of a subset of fine particles called nanoparticles (diameter < 50 nm) (3). The chemistry of nanoparticles may be worthy of special concern because some laboratory studies suggest an even stronger link between adverse health effects and smaller particles (4-7), and the strength of the response depends on composition (6). If it is concluded that nanoparticle

emissions should be reduced then a knowledge of nanoparticle composition will also be important for understanding the physical and chemical mechanisms by which they are formed. Such information is necessary to help establish criteria for engine design, operation, and fuel and lubricating oil compositional modifications that would help reduce nanoparticle formation. Unfortunately, due to the small size and low mass concentration of nanoparticles, chemical analysis of these species is difficult.

In an effort to further understand the problem of nanoparticle formation and develop reliable sampling and measurement techniques, the Coordinating Research Council is funding a research project (RFP E-43) headed by the University of Minnesota Center for Diesel Research (UMNCDR), titled "Diesel Aerosol Sampling Methodology."

The major objectives of the CRC RFP are to:

- 1) Determine actual particle size distributions and particle number concentrations in the exhaust plume from heavy diesel vehicles operated on the road.
- 2) Compare that information with data generated in emission test facilities to determine if current sampling and analysis methods are adequate for characterizing particle size.
- 3) Examine particle transformations as the plume disperses downwind of the roadway in a typical urban situation. The goal of this objective is to determine the zone of influence of the ultrafine particle fraction of the emissions from the roadway.
- 4) Characterize the bulk diesel particulate matter chemical composition and to determine surface properties and composition.

The general approach that is being used to meet these objectives is to first employ a mobile laboratory to measure the particle size distributions and number concentrations in the on-road exhaust plume from diesel test vehicles (two each from Cummins and Caterpillar), and then carry out laboratory experiments using a mini-dilution system and wind tunnel facility to reproduce these distributions when the same vehicles/engines are run under similar operating conditions on a chassis dynamometer. In addition, a number of techniques will be employed to obtain information on the chemical composition of the aerosol. The results of these experiments will be used to determine the major processes that influence the size distribution and number concentration of diesel exhaust particles, and to develop laboratory measurement techniques that will yield size distribution and concentration data that are representative of the on-road conditions. The results of the on-road measurements will also be used in models for understanding plume dispersion.

An important weakness in that study is that although one of the major objectives of the study is to determine the chemical composition of diesel particles, most of the aerosol measurements being made characterize physical properties of the particles, including the size distribution, number concentration, and surface area. The only real-time information on particle composition come from a photoelectric aerosol sensor that is used to measure the total mass concentration of polycyclic aromatic hydrocarbons (PAH). Some off-line chemical analyses for elemental and organic carbon, sulfate, and metals in particles collected using a microorifice

uniform deposit impactor (MOUDI) are also planned. It is also possible that gas chromatography-mass spectrometry (GC-MS) analysis will be performed to obtain more detailed information on organic speciation. Organic speciation studies of diesel exhaust particles have been conducted previously and usually involve filter collection of fine particles, with subsequent solvent extraction and GC-MS analysis with and without derivatization (8-12). Because of the complexity of the mixture only ~5-10% of the elutable particulate organic mass is amenable to speciated analysis (10, 11). Size-segregated diesel exhaust particles have also been collected using a MOUDI (13) and an electrical low-pressure impactor (ELPI) (12, 14) and analyzed for total organic and elemental carbon, sulfate and nitrate, and metals. The last stage of the MOUDI (15) is designed to collect particles with aerodynamic diameters between ~50-80 nm, and the ELPI ~30-70 nm. Particles smaller than the lowest cut-point are collected downstream on an afterfilter. In practice, diesel nanoparticle samples collected using these devices are subject to artifacts for a couple of reasons. Impactor stages having cut-points smaller than the mass median diameter of the sampled aerosol are particularly prone to errors associated with particle bounce. This is because bounce of a small fraction of particles from larger stages can add significantly to the mass collected on the nanoparticle stage. In addition, the aerodynamic size of diesel chain agglomerates is much smaller than their mobility equivalent size. A recent investigation by the Kittelson group of MOUDI performance with diesel particles found much higher than expected concentrations of particles larger than 100 nm electrical mobility diameter downstream of the 56 nm stage of the MOUDI. This is believed to be due to a combination of particle bounce and the low effective densities of carbonaceous agglomerates. Similar conclusions have been drawn from diesel particle density measurements made using an ELPI and scanning mobility particle sizer (12). Therefore, particles collected on nanoparticle impactor stages may contain relatively large chain agglomerates as well as small droplets formed by condensation. Other sampling artifacts that arise during impactor sampling are adsorption of vapors and volatilization of collected particles (13, 16). Although previous studies provide important insight into the chemical makeup of diesel particles, they lack reliable information on nanoparticle composition.

In an attempt to obtain compositional information on “clean” nanoparticle samples, the project described here is using a nano-differential mobility analyzer (Nano-DMA) (17) to size-select nanoparticles produced from diesel engine exhaust for subsequent chemical analysis by thermal desorption particle beam mass spectrometry (TDPBMS) (18-21). The Nano-DMA provides high concentrations of size-selected nanoparticles without significant contamination from larger particles. The TDPBMS has been used previously for real-time quantitative analysis of the organic composition of aerosols within the ~20-500 nm particle diameter size range (19).

### **3. OBJECTIVES**

The primary objective of Phase 1 was to evaluate the use the Nano-DMA/TDPBMS to obtain information on the chemical composition of diesel nanoparticles formed under various engine operating conditions. The studies were carried out at UMNCDR. The focus was on the chemistry of nucleation-mode particles, but larger particles were also analyzed for comparison. The goal was to use the composition data in conjunction with measured particle physical properties (e.g., size, concentration, etc.) to develop an understanding of the chemical mechanisms by which nanoparticles are formed in diesel exhaust. Such knowledge could aid in

determining modifications in engine design, operation, fuel, lubricating oil, or after-treatment that might be made in order to ameliorate the problem of nanoparticle formation.

The specific objectives of this seven-month research program were to:

- 1) Optimize operation of unipolar charger /Nano-DMA apparatus for obtaining size-selected diesel nanoparticles for TDPBMS analysis under various engine operating conditions.
- 2) Characterize particle beam focusing properties of aerodynamic lenses with spherical and diesel nanoparticles in order to determine size-dependent sampling efficiencies and gain information on diesel particle shape and its potential effect on sampling bias.
- 3) Characterize particle focusing properties of electrostatic and/or electrodynamic lenses with nucleation-mode size (<20 nm diameter) diesel nanoparticles in order to determine whether this lens system can improve the efficiencies with which nucleation-mode diesel particles can be sampled into the TDPBMS.
- 4) Determine the detection limits for TDPBMS analysis after the addition of an energy analyzer and new vaporizer.
- 5) Investigate the ability of temperature-programmed TDPBMS to analyze diesel fuel and lubricating oil, and investigate the use of high vaporization cell temperature and high electron energy to enhance the real-time TDPBMS signal intensity of PAHs relative to other species.
- 6) Use the Nano-DMA/TDPBMS to obtain real-time mass spectral/chemical composition data on diesel nanoparticles under various engine operating conditions.
- 7) Use temperature-programmed TDPBMS of collected size-selected particles to identify compounds present in diesel exhaust nanoparticles of complex composition. These measurements can also be used to estimate compound vapor pressures.
- 8) Identify the major PAHs in size-selected diesel nanoparticles by using high vaporization cell temperature and high electron energy to enhance the real-time Nano-DMA/TDPBMS signal intensity of PAHs relative to other species.

Objectives 1-3 were to be addressed by Professor Peter McMurry and coworkers at UMN, objectives 4-5 by Professor Paul Ziemann and coworkers at UCR, and objectives 6-8 involved measurements made with the combined Nano-DMA/TDPBMS and the participation of both research groups.

## 4. APPROACH

The research program was designed to accomplish the objectives through a combination of instrument development and characterization studies at UMN and UCR, followed by a diesel particle emission study at UMNCDR. If Phase 1 was successful, it was planned that Phase 2 would take place. This would involve participation in the Caterpillar study in Summer 2000 as part of the “Diesel Aerosol Sampling Methodology” study, and measurements in 2001 at the Cummins facilities.

## 5. RESULTS

### 5.1. PROJECT PERSONNEL

The faculty, postdocs, graduate students, and staff who participated in this project are:

University of California, Riverside (UCR):

Professor Paul Ziemann (PI)

Dr. Herbert Tobias (postdoc)

Derek Beving (graduate student)

University of Minnesota (UMN):

Professor Peter McMurry (subcontractor)

Dr. Hiromu Sakurai (postdoc)

Miriam Zuk (graduate student)

Professor David Kittelson (collaborator and director of CDR)

Robert Waytulonis (associate director of CDR)

Darrick Zarling (senior engineer at CDR)

### 5.2. PRELIMINARY RESEARCH AT UCR AND UMN

Because funding for the project was delayed until early February, 2000, it was not possible to complete all the planned preliminary work prior to the March study at UMNCDR. The following work was performed.

#### 5.2.1. Ziemann Group Experiments at UCR

In preliminary work for this project a tandem energy analyzer and a newly-designed vaporization cell were added to the TDPBMS and their impact on detection limits determined. The energy analyzer reduced background noise by a factor of ~100, and signal by a factor of ~3, resulting in an enhancement in signal-to-noise of ~30. The new 45° angled vaporizer did not enhance signal, and since the previous V-shaped design is less prone to losing particles by bounce, the V-shaped design was used in all later studies. Laboratory-generated aerosols of diesel fuel and lube oil provided by Professor Kittelson at UMN were analyzed using both the real-time

TDPBMS and temperature-programmed TDPBMS (TPTD) techniques. The TPTD was performed at a ramp rate of  $\sim 1^{\circ}\text{C}/\text{min}$ . All samples desorbed over a broad range of temperatures, with the lube oil being less volatile than the fuel. Mass spectra of individual compounds could not be resolved, but the mass spectra of the whole sample was similar for fuel and oil, and were indicative of a few classes of hydrocarbons. It had been planned that laboratory-generated, mixed PAH/organic aerosols would be analyzed with the TDPBMS at high vaporization temperature and electron energy in order to selectively fragment hydrocarbons so that more stable PAH could be observed, but time constraints did not allow for these experiments.

### **5.2.2. McMurry Group Experiments at UMN**

In preliminary experiments at UMN a unipolar charger/Nano-DMA was used to sample diluted diesel nanoparticles over a range of aerosol and sheath flow rates (these parameters set the resolution of the instrument) to determine optimum conditions for obtaining high nanoparticle concentrations in desired size ranges. In other experiments an electrostatic lens which had been designed to focus nanoparticles into the TDPBMS was evaluated. The previous design work was carried out computationally using the SIMION 3D program as part of a project funded by DOE. A key issue to be accounted for in the design was that focusing efficiency was determined by the distribution of the particles' kinetic energy, which we measured experimentally and found to be quite broad. This is presumably because there is a relatively broad distribution of particle masses even for DMA-classified particles and because particle acceleration through the pressure-reducing nozzle depends on radial location. SIMION calculations showed focusing is substantially degraded if the kinetic energy of a particle is smaller or larger than that for which the lens geometry and voltage settings are optimized. This problem was overcome by adding an electrostatic field parallel to the particle beam to accelerate particles to a uniform kinetic energy before they entered the focusing electrostatic field. A lens with such a pre-acceleration stage was constructed and tested with monodisperse 8 nm particles generated with an electrospray by measuring the particle current reaching a Faraday cup inside a particle beam apparatus. It was observed that with proper adjustment of the lens voltages a 6-7 times enhancement in signal could be obtained, indicating significant focusing.

### **5.3. DIESEL NANOPARTICLE STUDY AT UMNCDR**

The diesel nanoparticle study took place at the UMNCDR in March 2000. Shipping from California, set-up, and preliminary testing took place between 3/3 and 3/16. Diesel particle measurements using the TDPBMS began on 3/17 and continued through 3/27. Measurements involving the Nano-DMA and Nano-SMPS were performed by the McMurry group and those involving the TDPBMS were performed by the Ziemann group. CDR staff were in charge of operating the engine, exhaust dilution system, and SMPS. During almost all of this period Professors Ziemann, McMurry, and Kittelson were in town and daily meetings were held with all those involved in the study, which made for excellent interpretation, coordination, and planning of experiments. Additional experiments on particle focusing with the electrostatic lens, additional TDPBMS calibration experiments, and diesel particle size distribution SMPS and Nano-SMPS measurements were performed from 3/28-3/31. Data analysis began during the study and continued through June. The UCR group analyzed the thermal desorption particle beam mass spectrometer (TDPBMS) data. A significant amount of time was spent searching for and reading

literature on diesel fuel, lubricating oil, and particle chemical composition and mass spectra in order to interpret the study results. The UMN group analyzed the nano-DMA size distribution data, which involved a great deal of effort because of the need to correct size distributions obtained using the unipolar charger for the effects of multiple charging. The Ziemann group took the lead in synthesizing the data, preparing a manuscript, and submitting it to CRC/ARB for review. Details of the methodology and results of the study are given below.

### **5.3.1. Shipping, Set-up, and Preliminary Testing**

In preparation for the study at UMNCDR a set of high quality, sturdy, wooden packing crates was constructed in the Chemistry Department Machine Shop at UCR. These were used to ship the UCR equipment to UMN. The equipment was transported by ground from UCR to LAX airport on 3/3 and shipped by Northwest Air Cargo to Minneapolis/St. Paul on 3/4. The equipment was picked up in Minneapolis, taken to UMN, and unpacked on 3/6. The TDPBMS was reassembled in the UMNCDR and was under vacuum by 3/7. Although there was no apparent damage to any of the UCR equipment during shipping, there were initial problems with the performance of the quadrupole mass spectrometer. Even after retuning the instrument, the resolution was found to be very poor, and from 3/7-3/9 Dr. Tobias was in regular contact with technical support at Extrel (the mass spectrometer manufacturer) as they trouble-shot the instrument software and hardware. This was a very time-consuming process, since every time the vacuum chamber was opened to get access to the mass spectrometer, the chamber became recontaminated and had to be evacuated and baked for a sufficiently long period to clean the chamber. Not until 3/9, when the quadrupole rods were removed from their housing, and it was found that they had come slightly loose from their mount, was the problem solved. The instrument, which had been baked (both at high temperature, 300°C, and low temperature, 100°C) as often as possible while trouble-shooting, was then baked continuously over the weekend. From 3/13-3/15 the instrument was again baked, aligned, and tested with organic calibration particles. Professor Ziemann arrived on 3/15 and remained until the diesel studies were completed on 3/26.

At the same time as the TDPBMS was being set-up at UMN the McMurry group was modifying the mount for the electrostatic lens system they designed, so that it could be precisely mounted inside the TDPBMS. They also set up a unipolar charger/Nano-DMA for sampling size-selected diesel nanoparticles into the TDPBMS, a scanning Nano-DMA for measuring diesel particle size distributions, and an electrospray nanoparticle generator for producing high concentrations of organic nanoparticles for testing the efficiency with which the unipolar charger/Nano-DMA/electrostatic lens system would provide nanoparticles to the TDPBMS.

A series of experiments was undertaken in which monodisperse sucrose particles in the size range 15-200 nm were sampled into the TDPBMS to determine the sensitivity of the technique as a function of particle size [sensitivity = (signal counts/s)/(pg of particles/cm<sup>3</sup> air sampled)]. Particles 40 nm and larger were generated using an atomizer/DMA and the 15 nm particles using electrospray. The TDPBMS sensitivity decreased slowly with decreasing particle size and then dropped rather significantly between 40 and 15 nm. This is because Brownian motion degrades the aerodynamic focusing of smaller particles and so the sampling efficiency decreases. The electrostatic lenses were designed to improve sampling efficiencies for particles smaller than ~15-20 nm, but unfortunately the real-time TDPBMS signal that could be generated for 15 nm particles was too small to see above the background. It was decided that the

collection/desorption experiments that would be necessary to gain sufficient signal for evaluating the lenses in the TDPBMS system would be too time-consuming to pursue at that time, and so the diesel experiments were begun and carried out with the lenses set at voltages appropriate for focusing 15 nm particles. The lens should also focus somewhat smaller particles, and larger particles would not be affected. Additional focusing experiments were performed at the end of the study, as described below.

### **5.3.2. Methods**

A schematic of the apparatus used in the diesel exhaust studies is shown in Figure 1. A John Deere 4045 TF250 diesel engine was used to generate diesel exhaust, followed by exhaust dilution using a variable residence time dilution system (VRTDS). Diesel exhaust particles were charged using either a unipolar or bipolar charger, size-selected using a nano-differential mobility analyzer (Nano-DMA), and then chemically analyzed using a thermal desorption particle beam mass spectrometer (TDPBMS).

#### 5.3.2.1. Diesel Engine and Operation

Diesel particles were generated using a direct injection, 4-cylinder, 4.5 liter displacement, 4-cycle, turbocharged John Deere model 4045 TF250 diesel engine that produced a peak torque of 350 N-m at an intermediate engine speed of 1400 rpm, which is generally used for short-duration work periods of heavy lifting or material handling. Experiments were performed at a constant engine speed of 1400 rpm at four power levels: 15% load (50 N-m), 25% load (88 N-m), 40% load (140 N-m), and 50 % load (175 N-m). The fuel was EPA on-highway DF2 with 410-ppm sulfur and the lube oil was John Deere +50 Supreme 15W-40 motor oil.

#### 5.3.2.2. Diesel Engine Exhaust Sampling

Since concentrations of nanoparticles are strongly influenced by dilution conditions (3, 22), particles were sampled under constant conditions that closely simulate those in the ambient environment by using a two stage air injector, variable residence time, micro-dilution system (VRTDS) previously described in detail (22, 23). Briefly, the VRTDS consists of a primary and a secondary dilution stage separated by a retractable sampling tube. The length of the tube can be adjusted to control the aerosol residence time and therefore the growth of particles by coagulation and condensation of organics before secondary dilution freezes the size distribution. The dilution ratio is determined from the measured ratio of exhaust to diluted exhaust NO<sub>x</sub> concentration.

Parameters were optimized for generation of high concentrations of nanoparticles with sufficient mass so that subsequent chemical analysis could be performed above the detection limits of the instrumentation downstream of the VRTDS. Diesel particles were sampled using a total dilution ratio of ~64, with a primary dilution ratio of ~16, a secondary dilution ratio of ~4, and a residence time of ~1700 ms in the primary dilution system.

#### 5.3.2.3. Particle Size Selection and Size Distribution Measurements

Downstream of the VRTDS three particle size modes were selected for chemical analysis by TDPBMS. We refer to these as the total-mode, large nano-mode, and small nano-mode. Total-

mode particles are those analyzed without size-selection, obtained by sampling directly from the VRTDS into the TDPBMS. Large nano-mode particles are those sampled from the VRTDS into a unipolar charger, followed by a Nano-DMA for size selection. The unipolar charger (24) charges nanoparticles with high efficiency because ions of only a single polarity are present, and it reduces particle loss by directing the flows of ions and charged aerosol in an electric field. A sheath flow can be added to increase throughput of small particles, but was not used because it dilutes the aerosol and is not necessary for the sizes sampled here. The high charging efficiency of the unipolar charger increases the concentration of charged particles and therefore the sensitivity of nanoparticle measurement, but also generates a significant number of larger, multiply charged particles that can pass through the Nano-DMA and contribute to the nanoparticle sample. These particles shift the sampled mass distribution to larger sizes. Small nano-mode particles are those sampled into a radioactive  $\text{Po}^{210}$  bipolar charger, followed by a Nano-DMA. Bipolar-diffusion chargers (25), which are the standard chargers used with most DMAs, are not as efficient as unipolar chargers because the presence of both positive and negative ions tends to neutralize the aerosol charge, resulting in a lower concentration of charged particles. While use of this charger yields fewer charged nanoparticles for analysis, it also reduces the contribution of larger, multiply charged particles to the nanoparticle sample. Nanoparticle samples obtained when this charger is used therefore have a lower average mass than those obtained with the unipolar charger.

A Nano-DMA (TSI Model 3085) (17) was used downstream of the unipolar and bipolar chargers for particle size selection. The Nano-DMA separates charged nanoparticles according to their electrical mobilities and can provide accurate, high-resolution, size selection of particles in the 3-60 nm diameter range. In a Nano-DMA, a short path length and high inlet flow are used to reduce particle residence time and improve nanoparticle throughput, since diffusional losses during aerosol transport are significant for nanometer size particles. For our application, however, high-resolution was sacrificed by operating the Nano-DMA with a broadened transfer function (aerosol to sheath flow ratio of 1/2) in order to increase the mass concentration of nanoparticles entering the TDPBMS. In all experiments the aerosol flow rate was 1.6 L/min, with ~0.1 L/min flowing to the TDPBMS and 1.5 L/min to a condensation particle counter (TSI Model 3025 CPC), and the sheath air flow rate was 3.0 L/min. Under these conditions the half-width of the size distribution is ~25% of the selected diameter. Tandem DMA measurements made by placing a second Nano-DMA downstream of the first showed no significant tailing of the transfer function into larger sizes. The only particles outside the selected size window that passed through the Nano-DMA were those with multiple charges.

The size distribution of particles entering the TDPBMS from the Nano-DMA was measured with a Nano-SMPS (scanning mobility particle sizer; i.e., a scanning Nano-DMA) consisting of a bipolar charger, Nano-DMA (TSI Model 3085), and CPC (TSI Model 3025). The same instrument was used to measure the size distribution from 3-60 nm for particles exiting the VRTDS. The aerosol flow rate in the Nano-SMPS was 1.5 L/min and the sheath air flow rate was 15 L/min. A flow recirculation loop was used for the sheath air and excess air flows to improve flow control. The size distribution of particles exiting the VRTDS in the 10-320 nm range was measured using a conventional SMPS consisting of a bipolar charger, a DMA (26, 27) similar in design to the TSI Model 3934, and a TSI Model 3010 CPC. The aerosol flow rate was 1.0 L/min and the sheath air flow rate was 10 L/min.

The particle mobility distributions measured with the Nano-SMPS and SMPS were inverted to obtain particle size distributions. The procedure included corrections for particle

charging, the DMA transfer function, particle loss by diffusion in the DMA, diffusional broadening of the transfer function, and the CPC counting efficiency. Details of the general inversion procedure are described in the literature (28). Data from experimental and numerical studies (17) were used to correct for size-dependent diffusional loss and transfer function broadening in the Nano-DMA, and CPC counting efficiencies were obtained from the TSI manual. The size-dependent charge fractions were calculated using Fuchs' theory for bipolar diffusion charging (29).

The Nano-SMPS scans of the size distribution of nanoparticles exiting the Nano-DMA extended up to 60 nm, which was large enough to capture the entire small nano-mode distribution (Fig. 2C), but not the entire large nano-mode distribution (Fig. 2B). The latter distribution was therefore calculated using the SMPS size distributions for 10-320 nm particles exiting the VRTDS, the measured Nano-DMA transfer function, and the size-dependent charge fractions calculated using Fuchs' theory (29) for unipolar diffusion charging in the transition regime ( $Kn \sim 1$ ). A value of  $1.4 \pm 0.1 \times 10^7$  s/cm<sup>3</sup> was used for the product of the ion concentration and charging time in the unipolar charger. This value gave good agreement between calculated size distributions and those measured by the Nano-SMPS from 3-60 nm. Ion property parameters were taken from Pui et al. (30). Our analysis indicated that doubly charged particles contributed the most mass to large nano-mode particles, typically 40-50%, that singly and triply charged particles each contributed ~20-25%, and that more highly charged particles contributed ~10%.

#### 5.3.2.4. TDPBMS Particle Sampling and Fast-TPTD Analysis

Techniques for real-time (19) and temperature-programmed thermal desorption (TPTD) (18, 20, 21) analyses of aerosols using TDPBMS have previously been described in detail, but are used with several modifications in hardware and procedure for this work. Particles are sampled into the TDPBMS through a 100 micron orifice at 0.075 L/min, which reduces the pressure from atmospheric to ~2 torr. Using aerodynamic lenses (31, 32), particles are then focused into a tight particle beam and transported through two flat-plate skimmers separating three differentially pumped chambers. They enter a high-vacuum chamber at a pressure of  $\sim 3 \times 10^{-7}$  torr and reach a particle vaporizer with ~40-100% efficiency. Vacuum is maintained by turbomolecular pumps mounted on each chamber and backed by an oil-free mechanical scroll pump to reduce organic vapor contamination. All focused particles impact onto the inside walls of a v-shaped molybdenum foil vaporizer that is attached to a copper rod and is situated just outside the mass spectrometer ionizer. The particles were either continuously vaporized for real-time analysis by resistively heating the foil at ~250°C, or cryogenically collected for fast-TPTD analysis by cooling the foil to -50°C using an external liquid nitrogen bath. The temperature is monitored using a chromel-alumel thermocouple placed in contact with the foil. The desorbing molecules are ionized by 70 eV electrons and mass analyzed using a MEXM 500 quadrupole mass spectrometer (ABB Extrel, Pittsburgh, PA) and detected using a conversion dynode/pulse counting detector. The mass spectrometer was recently equipped with a tandem energy analyzer (ABB Extrel, Pittsburgh, PA) that reduced background noise by a factor of ~100 and signal by a factor of ~3, resulting in a signal-to-noise (S/N) improvement of ~30 over previous operation.

It is important to address two potential concerns about the TDPBMS technique. One is that the particle transport efficiencies may be lower than 40-100% if the diesel particles are not spheres, because lift forces lead to broader beams (31, 32) and increased losses at the skimmers

and the vaporizer. The gradual decrease in transport efficiency with decreasing particle size in this range will only bias the composition of the collected sample slightly toward larger particles, and so should not effect the qualitative results. In the extreme case that the nanoparticle aerosol consists of a mixture of spherical and highly irregularly-shaped particles having very different compositions, then the effect of shape on sampling could be more significant. A second concern is the possible evaporation of particles prior to collection on the cold vaporizer. Evaporation does not occur from the  $-50^{\circ}\text{C}$  substrate, but we have shown previously (19) that particulate compounds with vapor pressures greater than  $\sim 10^{-5}$  torr can evaporate prior to reaching the vaporizer leading to loss of the more volatile aerosol components. In the present study we have detected compounds with vapor pressures as high as  $\sim 10^{-4}$  torr. Furthermore, on the basis of gas-particle partitioning theory compounds with vapor pressures higher than  $\sim 10^{-4}$  torr will be predominantly in the gas phase, so collecting more volatile compounds is not an important issue.

Total-mode diesel particle signal was below the detection limits of the TDPBMS when sampled in real-time so only TPTD was used for chemical analysis. In previous studies, TPTD was used to separate, identify, and estimate vapor pressures of individual compounds in laboratory-generated aerosols comprised of a few components. In this work, slightly longer particle collection times and an  $\sim 100$  times faster desorption rate were used to enhance S/N over that of real-time analysis. This allowed us to identify and estimate the vapor pressures of a few compound classes in the diesel particles, which are comprised of many components. We refer to this analytical procedure as fast-TPTD. Particles sampled from a particular size mode were cryogenically collected onto the cold foil for times varying from 15-70 min. After collection, the components of the sample were quickly desorbed according to their vapor pressures and therefore separated to some degree in time. During desorption, the foil was resistively heated from approximately  $-50$  to  $+300^{\circ}\text{C}$  over 6 min using a fixed current from a high-current power supply. The nonlinear temperature ramp rate was about 150, 100, and  $50^{\circ}\text{C}/\text{min}$  in the first, second, and third minutes and then reached a plateau of  $\sim 300^{\circ}\text{C}$  over the remaining 2-3 minutes. Throughout the desorption period the mass spectrometer samples a portion of the evaporating molecules for mass analysis. Signal due to background gases was determined by sampling diesel exhaust under the same conditions as for the small nano-mode and large nano-mode particles, except that the Nano-DMA was set at 0 volts to allow only diesel exhaust gases to pass. Background gases at 50% load were cryogenically collected for 1-2 hours and then analyzed using the fast-TPTD procedure. Particles generated at each of the four engine conditions (15%, 25%, 40%, 50% load) were sampled from the three size modes and analyzed using fast-TPTD.

#### 5.3.2.5. Mass Spectral Analysis: Full Scan or Five-Mass SIM

Mass spectral analysis of collected particles was conducted either by continuous scanning over an appropriate mass range or by single-ion monitoring (SIM) of five mass-to-charge ratios ( $m/z$ ). Mass spectra were scanned from  $m/z$  45-300 or  $m/z$  45-480 at scan rates of 7 to 30 s, with 1 amu step size, and with detector dwell times of 25 or 50 ms at each  $m/z$ . Particle samples for full mass spectral analysis were collected for 35-70 min depending on particle mass flux. Sampling times increased as the mass decreased from the total-mode to the small nano-mode.

For certain sampling conditions (e.g., small nano-mode, 50% load), too little nanoparticle mass was collected in 70 min for full mass spectral analysis. Increasing collection times wasn't feasible, so instead, SIM of five  $m/z$  signals was used to enhance S/N. This allowed for longer dwell times (3000 ms) at each mass, compared to the scanning mode (25-50 ms), and provided

sufficient S/N to distinguish low nanoparticle signal from background. The enhanced S/N also produced better-defined desorption profiles ( $m/z$  signal versus temperature) than were obtained with the mass-scanning method, thereby improving estimates of compound vapor pressures based on desorption temperatures. The five masses used in the SIM method were chosen to represent hydrocarbons and sulfuric acid:  $m/z$  69 for cycloalkanes,  $m/z$  85 for alkanes,  $m/z$  95 for “non-specific” hydrocarbons, and  $m/z$  81 and 98 for sulfuric acid. Diesel particles were collected for 60 min for all fast-TPTD analyses performed using the SIM method. The estimated mass of collected particles increased from 3 to 14 ng for the large nano-mode and 0.5 to 0.8 ng for the small nano-mode as the engine load decreased from 50 to 15%. These values were calculated assuming particle transport efficiencies of ~90% for the large nano-mode and ~60% for the small nano-mode, based on measurements made previously with dioctyl sebacate (19). The total-mode mass was not estimated because of the incomplete size distribution data. The estimated detection limit for a 60 minute collection time and fast-TPTD/SIM analysis for  $m/z$  69, 81, and 95 is ~0.2 pg for large nano-mode particles, which corresponds to a concentration of ~0.05  $\mu\text{g}/\text{m}^3$  in the flow exiting the Nano-DMA. The detection limit for the same  $m/z$ 's for small nano-mode particles is ~0.5 pg, equivalent to a concentration of ~0.1  $\mu\text{g}/\text{m}^3$ . Estimated detection limits for  $m/z$  85 and 98 are approximately 2 and 8 times greater than the other three masses in both modes.

#### 5.3.2.6. TDPBMS Calibration and Standards Analysis

The TDPBMS was calibrated with standard compounds so that relative concentrations and vapor pressures of the diesel particle components could be estimated. Aerosol standards were generated using a Collison atomizer (33). A solution of ~0.1% (w/w) pure organic compound, diesel fuel, or lubricating oil in hexane, or ~1% (w/w) ammonium sulfate or ~2% (w/w) concentrated sulfuric acid in water was atomized using clean air and sent through either an activated charcoal or silica gel diffusion drier to evaporate hexane or water solvent, respectively. The submicron dried aerosol was then passed through a bipolar charger and DMA to select ~100 nm particles. The particle current exiting the DMA was measured using a Faraday cage and electrometer to determine the particle concentration, which was used with the known size, density, and sampling rate to calculate the particle mass flux (19). Approximately 3-5 ng of aerosol was cryogenically collected on the foil in the TDPBMS high-vacuum chamber and then analyzed using the same fast-TPTD procedure as for diesel particles. Mass spectral analysis was performed by scanning from  $m/z$  45-100 for sulfuric acid and ammonium sulfate and  $m/z$  45-300 for fuel and lubricating oil standards. Pure organic standards were analyzed using SIM of  $m/z$  85 for the n-alkanes hexadecane [ $\text{C}_{16}\text{H}_{34}$ ], eicosane [ $\text{C}_{20}\text{H}_{42}$ ], tetracosane [ $\text{C}_{24}\text{H}_{50}$ ], octacosane [ $\text{C}_{28}\text{H}_{58}$ ], and dotriacontane [ $\text{C}_{32}\text{H}_{66}$ ], and  $m/z$  95 for cholestane [ $\text{C}_{27}\text{H}_{48}$ ]. Some standards were also analyzed in real-time while scanning from  $m/z$  45-300.

#### 5.3.2.7. Materials

All chemical standards were obtained from Aldrich Chemical Co, Inc. and were used without further purification. All solvents were obtained from Fischer Scientific. The commercial EPA on-highway DF2 fuel with 410-ppm sulfur and the John Deere +50 Supreme 15W-40 motor oil was provided by Professor Kittelson at UMN.

#### 5.3.2.8. Electrostatic Focusing Experiments

At the end of the diesel study, experiments were performed to more thoroughly evaluate the performance of the electrostatic lens system for focusing particles smaller than those analyzed in the diesel study. Monodisperse 15 nm dioctyl sebacate and sucrose nanoparticles were sampled into the TDPBMS, collected on the vaporizer, and then flash-desorbed ( $\sim 0.1$  s) using a fast-pulse power supply. Unfortunately, the signal was low and the background fluctuated too much to allow for an accurate determination of focusing behavior. The increase in signal obtained by using the electrostatic lenses to focus nanoparticles inside the TDPBMS is therefore uncertain at this time.

### 5.3.3. Results

#### 5.3.3.1. Experimental Matrix

A summary matrix of the engine conditions and size distribution properties of the aerosol samples analyzed by fast TPTD is given in Table 1. Examples of number and mass distributions calculated from the SMPS and Nano-SMPS measurements are shown in Figure 2 for each of the three particle size modes. Mass distributions were calculated assuming unit density spheres. The mass distributions were used to calculate for each sample the mass median diameter, MMD (i.e. the diameter for which half the mass is contributed by particles smaller than MMD and half by larger particles). For these calculations the concentrations of large nano-mode particles beyond 60 nm not measured by the Nano-SMPS were estimated using the procedure described above. The MMD of the total-mode particles is not known because SMPS scans stopped at 320 nm before reaching the upper end of the size distribution. The total size distribution in Figure 2A shows a bimodal structure with a “nuclei mode” with a MMD in the nanoparticle range and an “accumulation mode” with a MMD in the 0.1-0.2  $\mu\text{m}$  range. The nuclei mode, which generally consists of mainly volatile materials (3), decreases with increasing load, presumably as a result of higher exhaust temperatures leading to more complete combustion of partially burned fuel and lubricating oil. On the other hand, the accumulation mode, which generally consists of solid carbonaceous particles (3), increases with increasing load as a result of more locally rich combustion zones associated with larger quantities of fuel injected into the cylinders. The number concentrations downstream of the VRTDS were  $\sim 1-3 \times 10^5/\text{cm}^3$  and the diameters at the number peak were  $\sim 17-21$  nm. The range of MMDs was  $\sim 38-58$  nm for the large nano-mode particles, and  $\sim 26-31$  nm for the small nano-mode particles. Notice that the number and mass distributions of the large nano-mode particles have clear contributions from singly and doubly charged particles because of the high efficiency of the unipolar charger, whereas the small nano-mode particles are predominantly singly charged by the bipolar charger.

### 5.3.3.2. Particle Mass Spectra

Because diesel particle emissions depend on the engine, operating conditions, fuel, and lubricating oil, results of diesel exhaust studies are often not directly comparable. However, general trends can be noted from past studies and applied to the analysis of this work. Full mass spectra were obtained at the signal maximum during desorption of large nano-mode particles for two different size distributions at 15% load (Figure 3A, 3B), and for total-mode particles at 50% load (Figure 3C). The mass spectra are similar, and so by themselves do not indicate an obvious dependence of chemical composition on particle size or engine load. Desorption profiles obtained using the five-mass SIM method, however, do reveal important compositional differences that will be discussed below. Mass spectra of the fuel and lubricating oil were also obtained using the same fast-TPTD analysis (Figure 4A, 4B) and are similar to the diesel particle spectra. This result suggests that unburned fuel and lubricating oil are a major source of the organic matter in diesel exhaust particles.

A number of other studies have shown that fuels and lubricating oils contribute to diesel exhaust particles (8-11, 34-36), usually in the form of unburned fuel and lubricating oil components, partially oxidized products from combustion of fuel and lubricating oil, pyrolysis products, and fuel/oil additive combustion products (10). Analysis of diesel fuels and lubricating oils reveal hydrocarbons that range from C10-C25 for fuels and from C14-C45 for oils (8-10, 37, 38), with varying relative contributions that depend on fuel/oil additives, and oil viscosity. Compounds common to both fuels and oils are n-alkanes (paraffins or waxes), branched alkanes, cycloalkanes (naphthenes), aromatics (mono and polycyclic aromatic hydrocarbons (PAH)), naphthoaromatics (aromatic rings fused with naphthenic rings and chains), and sulfur, nitrogen, and oxygen containing compounds (8-10, 37, 38). Fuels normally contain high concentrations of n-alkanes, while lubricating oils contain high concentrations of cycloalkanes and naphthoaromatics, due to significant reductions of n-alkanes and slightly branched isoalkanes from commercial dewaxing processes (39). Thermocracking of the heavy distillates in lubricating oils results in the formation of n-alkanes, indicating that the distillates contain a significant fraction of cycloalkanes with n-alkyl side-chains of various lengths. This general compositional difference is reflected in the mass spectra of the fuel and lubricating oil used in this work. For instance, the mass spectrum of the fuel is enriched in n-alkanes and branched alkanes ( $m/z$  85) relative to cycloalkanes ( $m/z$  83), while the mass spectrum of the oil is enriched in cycloalkanes.

Previous studies of diesel exhaust particles involved filter and impactor collection of fine particles, solvent extraction, and gas chromatography-mass spectrometric (GC-MS) analysis with and without derivatization (8-11, 13, 40). Using these techniques ~5-10% of the elutable particulate organic mass was amenable to speciated analysis (10, 11), leaving the remaining elutable organic mass as an unresolved complex mixture (UCM). Rogge et al. determined that the UCM consisted mainly of branched and cyclic hydrocarbons (10) and Schauer et al. found the UCM to be similar to motor oil. It was found that about ~30-40% of the fine particle mass was organic carbon, another ~30-40% was elemental carbon, and the remainder was unknown (11, 13, 40). The composition of the 5-10% fraction of particulate organic mass “resolved” using GC ranged from ~20-60% alkanes, ~20-30% n-alkanoic and alkanedioic acids, 4-40% PAH, and < 4% each of benzoic acids, oxy-PAH, hopanes, steranes, and other compounds, such as those containing nitrogen (10, 11). If the TDPBMS were used to analyze these particles elemental carbon, metals, and refractory inorganics would not be detected because the maximum vaporizer temperature is too low to vaporize these species. Organics, mostly UCM (>90%), would

contribute to the mass spectrum. Evidence for “trace” compounds (<1%) would probably be buried in the UCM portion of the TDPBMS mass spectrum.

The diesel particle mass spectra acquired in this work (Figure 3A-3C) show an intense series of peaks at  $m/z$  57, 71, 85, 99, 113, 127, 141,... which are indicative of normal and branched alkanes. Another strong set of peaks at  $m/z$  55, 69, 83, 97, 111, 125, 139,... are indicative of cycloalkanes, especially alkyl-substituted monocyclic alkanes. The types of compounds found in lubricating oil and fuel generally have a long alkyl side-chain and may or may not also have small side-chains (41). A number of cyclohexanes, such as hexadecylcyclohexane, have been identified in filter-collected diesel particles using GC-MS (11). Generally, one of the most intense peaks in alkyl-substituted cyclohexane mass spectra is  $m/z$  83 (42). Methyl groups on the ring increase the mass of the fragment ion in units of  $\text{CH}_2$ , leading to peaks at 97, 111, ... The mass spectra of particles in all modes have a greater relative abundance of  $m/z$  83 than  $m/z$  85, indicating that the diesel particles are slightly more enriched with cycloalkanes than alkanes, and therefore resemble the lubricating oil more than the fuel. Oils have low amounts of n-alkanes, so  $m/z$  85 may represent mostly branched alkanes. Alkyl-substituted cycloalkanes and branched alkanes are probably the largest contributor to the diesel particle organic composition, as indicated by our results and past studies in which most of the UCM particulate mass was composed of these compound classes (9-11).

In addition to the series of peaks from alkanes and cycloalkanes mentioned above, there is a major series of peaks at  $m/z$  67, 79, 81, 95, 107, 109, 121, 123, 135, 149, 151... that can have contributions from many “non-specific” sources, but still represents cyclic and branched hydrocarbons. This is characteristic of the mass spectra of UCM (43). For example,  $m/z$  149 is a common fragment from cyclic hydrocarbons that have at least 2 or more rings, and some of the lower mass peaks also have contributions from these compounds.

The series of peaks at  $m/z$  77, 91, 105, 119, 133... indicate a significant contribution from aromatics such as alkyl-substituted benzenes. Terpanes with 3 and 5 rings (hopanes) mostly give rise to  $m/z$  149, 177, and/or 191, which are observed in the diesel particle mass spectra and indicate that hopanes may be present in small quantities. The series of peaks at  $m/z$  67, 81, 91, 93, 95, 107, 109, 121, 135, and 149 are also present in the mass spectrum of cholestane, but the absence of a very intense marker at  $m/z$  217 indicates that steranes could only be present in trace amounts. Past studies have detected hopanes and steranes in low concentrations, and they are often used (along with pristane and phytane) as unique molecular markers for fingerprinting petroleum residues in atmospheric aerosols (8, 9, 44-47). Past studies have also identified significant amounts of n-alkanoic and alkanedioic acids in the elutable portion of diesel particles, but the very low signal at  $m/z$  60, which is a major peak in the spectra of these acids, indicates that only trace quantities could be present in our particles.

Because of their classification as probable human carcinogens, polycyclic aromatic hydrocarbons (PAH) have been the focus of many studies of diesel exhaust particle composition (48-51). PAH are very stable, and the mass spectra essentially contain only the molecular ion, which makes identification of the compounds straightforward. The molecular weights of some of the major PAH up to 250 amu are 128 (naphthalene), 178 (phenanthrene), 202 (fluoranthrene and pyrene), and 228 (benz[a]anthrene and chrysene) (52). Although signal is present at these masses in our diesel particle spectra, none of the peaks stand out above neighboring peaks. Therefore, it can only be said that if PAH are present, their contribution to the overall particulate mass is small. This conclusion is in agreement with the percentage of PAH found in total elutable particulate mass in previous studies (10, 11).

### 5.3.3.3. Effect of Engine Load and Particle Size on Composition and Volatility of Organic Aerosol

At high engine load the nanoparticle mass collected in 60 min was too low for full mass spectral analysis. Selected ion monitoring (SIM) of only five masses was therefore used instead to achieve greater S/N. The  $m/z$  69 peak was chosen to represent cycloalkanes,  $m/z$  85 was chosen for alkanes, and  $m/z$  95 was chosen for “non-specific” hydrocarbons. In addition,  $m/z$  81 and 98 were monitored to look for evidence of sulfuric acid. Figure 5 shows the mass thermograms ( $m/z$  signal versus vaporizer temperature) of  $m/z$  69 from fast-TPTD experiments performed using the five-mass SIM method. These plots provide information on the relative volatilities of the particle components, since lower volatility compounds desorb at higher vaporizer temperatures. Analysis of total-mode particles at 15% load reveals a single peak in the  $m/z$  69 signal at 37°C (Figure 5AI), while those at 50% load (Figure 5DI) peak at 107°C. The total-mode desorption profiles at 25% (Figure 5BI) and 40% (Figure 5CI) load show two distinct peaks. A commonly used method to determine the relative contributions of fuel and lubricating oil to the total organic extractable fraction of diesel particles is to measure the equivalent carbon number distribution of the extracts using a gas chromatograph. The resulting distribution usually has two distinct peaks with the lower corresponding to fuel and the upper lubricating oil (8). This may be the explanation for the bimodal profiles seen in Figures 5BI and 5CI. Analyses using  $m/z$  85 and 95 (Figures 9 and 10) show the same general trend as for  $m/z$  69: the desorption peaks of the organic markers shift to higher temperature as engine load increases, indicating a decrease in average organic compound volatility. As engine load increases, the more volatile fuel component is burned, leaving the lubricating oil component as the principal peak. These heavier, less volatile compounds appear to be the principal components of the nanoparticles.

At the engine loads studied here the desorption peaks in the five-mass SIM analyses shift to higher temperatures with decreasing particle size. For example, at 15% load total-mode particle signal at  $m/z$  69 peaks at 37°C (Figure 5AI), while small nano-mode particle signal peaks at 170°C (Figure 5AIII). Analyses using  $m/z$  85 and 95 reveal the same trend. This large temperature change is indicative of a large decrease in average organic compound volatility with decreasing particle size. In general, as the engine load increases and/or particle size decreases, the particle composition shifts to heavier organics, heavier in fact than the average for the lubricating oil used in this work. The observed size dependence is consistent with the Kelvin effect and particle growth theory, as will be discussed below.

Because of the extensive fragmentation that occurs from electron ionization, and the similarity in mass spectra of compounds in the same classes, it was not possible to determine the average molecular weights of the organic aerosol components from TDPBMS mass spectra. Instead, a series of n-alkane standards was analyzed using fast-TPTD and the average carbon number (equivalent to molecular weight) and vapor pressure of diesel components were estimated from plots of  $\log(\text{vapor pressure})$  and carbon number versus  $(\text{desorption temperature})^{-1}$  (Figure 6). The vapor pressures of hexadecane, eicosane, tetracosane, octacosane, and dotriacontane at 25°C were taken from the literature (53-55). The plots for vapor pressure and carbon number are nearly identical because  $\log(\text{vapor pressure})$  depends linearly on carbon number. The plots are nonlinear because of the nonlinear temperature ramp rate employed in the fast-TPTD analyses. A  $\log(\text{vapor pressure})$  versus  $(\text{desorption temperature})^{-1}$  correlation for mono- and di-carboxylic acids obtained previously using a much slower, linear ramp rate was

linear (18). Using the plot in Figure 6, the average carbon number of the alkanes at the 37°C desorption peak for total-mode particles at 15% load is estimated to be  $\sim C_{17}$ , corresponding to a vapor pressure of  $\sim 2 \times 10^{-4}$  torr. At higher engine loads and smaller particle sizes a typical desorption temperature is  $\sim 170^\circ\text{C}$ , which corresponds to  $\sim C_{24}$  and  $\sim 5 \times 10^{-8}$  torr. Fuel and lubricating oil standards desorb at 25°C and 72°C (Figures 8A, 8B), respectively, indicative of the more volatile, lower molecular weight composition of the fuel ( $\sim C_{17}$  or  $\sim 2 \times 10^{-4}$  torr vapor pressure) compared to the lubricating oil ( $\sim C_{19}$  or  $9 \times 10^{-5}$  torr vapor pressure). Total-mode particles at 15% engine load desorb at an average temperature of  $\sim 35^\circ\text{C}$ , suggesting that at that load the overall chemical composition of diesel particles is similar to the fuel.

#### 5.3.3.4. Evidence for Sulfuric Acid in Nanoparticles

During combustion most of the sulfur in diesel fuel is oxidized to  $\text{SO}_2$  and a few percent is further oxidized to  $\text{SO}_3$ , which subsequently reacts with water to form sulfuric acid (14, 23). Sulfuric acid has a low vapor pressure (especially in the presence of water vapor), and small amounts have been measured in diesel particles. For example, the mass of sulfate was  $\sim 6\%$  of the total in 30-73 nm particles sampled from a diesel engine operated on high-sulfur fuel ( $\sim 400$  ppm S) (14), and  $<1\%$  in 45-80 nm particles when low-sulfur fuel ( $\sim 30$  ppm S) was used (13). It has been proposed that sulfuric acid is the nucleating agent in diesel nanoparticle formation (14, 23), but this has not been convincingly demonstrated. For this reason, two of the five SIM peaks,  $m/z$  81 and 98, were used to search for evidence of sulfuric acid in diesel nanoparticles. These peaks were chosen because they were the largest in the fast-TPTD mass spectrum of the standard (Figure 4C) and weren't significantly affected by background gas signal, as were  $m/z$  48 and 64. The subsequent discussion of trends will refer to Figure 8, which shows results for  $m/z$  98. The behavior of  $m/z$  81 is similar and is shown in Figure 11. For all engine conditions and size modes the organic mass spectral peaks  $m/z$  69, 85, and 95 desorb over the same temperature ranges and exhibit the dependence on particle size and engine load described above. At 15% load, the  $m/z$  81 and 98 desorption profiles for all three size modes ( $m/z$  98 is shown in Figures 8AI-8AIII) contain a single peak at the same temperature as  $m/z$  69, 85, and 95, indicating an organic contribution to these  $m/z$ 's. Similar behavior is observed for the total-mode particles at 40% and 50% load (Figures 8CI, 8DI), but the desorption profiles of the large nano-mode particles at these loads are very different: although  $m/z$  69, 81, 85, 95, and 98 all have a peak at  $\sim 150$ - $180^\circ\text{C}$ , a distinct second peak appears in the desorption profiles of  $m/z$  81 and 98 at  $\sim 22$ - $43^\circ\text{C}$  (Figures 8CII, 8DII). A sulfuric acid standard analyzed using fast-TPTD desorbed at  $\sim 30^\circ\text{C}$  (Figure 7C), supporting the idea that this second peak is due to sulfuric acid. The sulfuric acid peaks are apparently masked at lower engine load and in larger particles by the presence of higher volatility organics that desorb at  $\sim 25$ - $39^\circ\text{C}$ . It is important to note that although pure sulfuric acid has a vapor pressure of  $\sim 10^{-5}$  torr (56), which is in reasonable agreement with the value determined from Figure 6, water vapor decreases the vapor pressure by orders of magnitude lower. Particles sampled into the TDPBMS probably contain a sulfuric acid-water solution, and the water evaporates inside the vacuum chamber.

The mass of sulfuric acid in diesel nanoparticles can be estimated using the mass spectral data. The assumptions are that the particles are composed of sulfuric acid and organics and that the mass fraction of sulfuric acid,  $X_{\text{H}_2\text{SO}_4}$ , is equal to

$$X_{\text{H}_2\text{SO}_4} = (I_{\text{H}_2\text{SO}_4}/I_{\text{AEROSOL}})(S_{\text{AEROSOL}}/S_{\text{H}_2\text{SO}_4}) \quad (1)$$

where  $I$  is the ion signal and  $S$  is the number of ions generated per unit mass. To calculate  $S$  we also assume that the sampling efficiencies into the mass spectrometer are the same for all molecules and ions. The aerosol ion signal is the total ion signal minus background gas signal, and  $S_{\text{AEROSOL}}$  is equal to an average value for organics, since they compose the bulk of the aerosol. The ionization cross sections of organics in a homologous series of compounds are proportional to the compound molecular weights, so that  $S$  is constant. Furthermore,  $S$  is similar for many organics (57). The ratio  $S_{\text{AEROSOL}}/S_{\text{H}_2\text{SO}_4}$  for 70 eV ionization estimated using a molecular total ionization cross section/molecular mass of  $\text{C}_6\text{H}_{14}$  equal to  $22 \times 10^{-16} \text{ cm}^2/86$  (58) for  $S_{\text{AEROSOL}}$  and  $7 \times 10^{-16} \text{ cm}^2/98$  for sulfuric acid is 3.6. The cross section of sulfuric acid is assumed to be equal to the values for  $\text{SO}_2$  and  $\text{H}_2\text{S}$ , which are approximately the same (58, 59). The value for  $\text{SO}_3$  is the same as that for  $\text{SO}_2$  at 30 eV (60), but the 70 eV value has not been reported. A value of 1.5 was measured for  $S_{\text{ORG}}/S_{\text{H}_2\text{SO}_4}$  in the laboratory using standard tetracosane and sulfuric acid aerosols, so the calculation  $X_{\text{H}_2\text{SO}_4}$  is performed for the range of values 1.5-3.6. The contribution of the  $m/z$  98 signal to the total ion signal obtained by summing the full mass spectra collected during the entire desorption period for large nano-mode particles at 15% load and total mode particles at 50% load ranges from 0.7-1.3%. We assume that the value for large nano-mode particles at 40% and 50% load is also in this range. This value is multiplied by the fractional contribution of sulfuric acid to the  $m/z$  98 signal, which is estimated to be 0.45 at 40 % load and 0.25 at 50% load from the relative areas of the peaks for sulfuric acid (peak  $\sim 30^\circ\text{C}$ ) and organics (peak  $>150^\circ\text{C}$ ) in the  $m/z$  98 mass thermograms (Figures 8CII, 8DII). This gives the fraction of the total ion signal contributed by the sulfuric acid  $m/z$  98 peak. The fraction of the total ion signal contributed by all sulfuric acid peaks,  $I_{\text{H}_2\text{SO}_4}/I_{\text{AEROSOL}}$ , is obtained by multiplying by 2.5 to account for the  $m/z$  48, 64, 80, and 81 peaks in the sulfuric acid mass spectrum (Figure 4C). Using the range of values and eq (1) we estimate that sulfuric acid makes up  $\sim 1.2$ -5.3% of the mass of the large nano-mode particles at 40% engine load. Similar calculations yield a value of  $\sim 0.7$ -2.3% at 50% load.

A reasonable model for these particles is that they consist of a core of sulfuric acid (and water, depending on the relative humidity) surrounded by an organic shell. A two-phase particle is expected since alkanes and other unreactive nonpolar hydrocarbons are insoluble in sulfuric acid (61), and the sulfuric acid should be on the inside of the particle since this configuration minimizes the free energy by minimizing the surface area of the component with the largest surface tension (sulfuric acid/alkane surface tension is  $\sim 2$ -3; CRC, 1983) (62). For such particles the diameter of the sulfuric acid core,  $D_{\text{H}_2\text{SO}_4}$ , can be calculated using the equations

$$\rho_{\text{PARTICLE}} = [(X_{\text{H}_2\text{SO}_4}/\rho_{\text{H}_2\text{SO}_4}) + (X_{\text{ORG}}/\rho_{\text{ORG}})]^{-1} \quad (2)$$

and

$$D_{\text{H}_2\text{SO}_4} = D_{\text{PARTICLE}}[(\rho_{\text{PARTICLE}} - \rho_{\text{ORG}})/(\rho_{\text{H}_2\text{SO}_4} - \rho_{\text{ORG}})]^{1/3}, \quad (3)$$

which can be derived from the conservation of particle volume and mass. The densities of sulfuric acid and organics are taken to be  $\rho_{\text{H}_2\text{SO}_4} = 1.8 \text{ g/cm}^3$  and  $\rho_{\text{ORG}} = 0.8 \text{ g/cm}^3$  for alkanes. For the large nano-mode particles at 40% engine load, which have a MMD of 41 nm, the calculations indicate a sulfuric acid core  $\sim 7$ -12 nm in diameter. At 50% load the MMD is 58 nm and the calculated sulfuric acid core is  $\sim 8$ -13 nm.

For large nano-mode particles at 25% engine load, in which  $m/z$  69, 81, 85, 95, and 98 all peak at temperatures higher than  $125^\circ\text{C}$ , a second peak at  $\sim 40^\circ\text{C}$  appears in the desorption

profiles of  $m/z$  69, 81, 95 and 98 (but not for 85). The source of this is probably higher volatility organic components present in the particles along with lower volatility ones. Unfortunately, the signals for  $m/z$  81 and 98 for the small nano-mode particles at 40% and 50% engine load were too low to make reliable estimates of the sulfuric acid contribution to these particles.

### 5.3.3.5. Mechanism of Diesel Nanoparticle Formation

The results of this study are consistent with a mechanism of diesel nanoparticle formation involving homogeneous binary nucleation of sulfuric acid and water followed by growth from condensation of organic species. This mechanism has been proposed previously and supported by computational models of nucleation and growth combined with measurements of the composition of size-segregated particles (14) and particle growth rates (23). All these studies were performed using fuel with a high sulfur content of  $\sim 400$  ppm S. The upper end of the  $\sim 0.7$ -5% range for sulfuric acid mass fraction estimated here for large nano-mode particles with MMDs of  $\sim 40$ -60 nm is close to the value of  $\sim 6\%$  estimated for  $\sim 30$ -73 nm diesel particles collected with an ELPI sampler (14). The corresponding sulfuric acid nucleus diameter range of  $\sim 7$ -13 nm is comparable to the  $\sim 8$  nm value for the sulfuric acid-water nucleus estimated from particle growth rates by Khalek et al. (23).

It is possible that the nucleating species is ammonium sulfate rather than sulfuric acid. The salt has a lower vapor pressure, and measurements of ambient new particle formation rates indicate that it may participate in atmospheric nucleation (63, 64). Ammonium concentrations in 45-80 nm MOUDI-sampled particles from a diesel engine run on low sulfur fuel ( $\sim 30$  ppm S) were sufficient to neutralize  $\sim 75\%$  of the  $\text{H}_2\text{SO}_4$  to  $(\text{NH}_4)_2\text{SO}_4$  (13). The TPTD desorption profile in Figure 7D for a mixture of sulfuric acid and ammonium sulfate particles shows that ammonium sulfate peaks at  $\sim 60^\circ\text{C}$ , which is significantly higher than sulfuric acid. Ammonium sulfate could contribute to the low-temperature peak in the  $m/z$  98 signal for large nano-mode particles (Figures 7C, 7D), but sulfuric acid appears to be the major sulfate-containing species.

It seems unlikely that organic compounds alone are nucleating. The desorption profiles of organics all approach the baseline at temperatures between  $\sim 250$ - $300^\circ\text{C}$ , which from extrapolation of the curve in Figure 6 indicates that the vapor pressures and carbon numbers of the least volatile organics are on the order of  $\sim 10^{-12}$ - $10^{-14}$  torr and  $\sim 34$ -38, respectively. These vapor pressures, which are for a flat surface at  $25^\circ\text{C}$ , are comparable to those above a sulfuric acid-water solution at this temperature and  $\sim 30$ -60% relative humidity (65). Because of the Kelvin effect, however, a small organic particle of this type would have a much higher vapor pressure than a sulfuric acid-water particle of the same size. For example, the Kelvin equation for a pure spherical particle is

$$P = P^0 \exp(4\sigma M / RT\rho D), \quad (4)$$

where  $P$  is the equilibrium vapor pressure of the compound above a particle of diameter  $D$ ,  $P^0$  is the equilibrium vapor pressure of the compound above a flat surface,  $\sigma$  is the surface tension,  $M$  is the molecular weight,  $R$  is the gas constant, and  $\rho$  is the particle density. Using values of  $\sigma = 30$  and  $70$  dyn/cm,  $M = 500$  and  $98$  g/mol, and  $\rho = 0.8$  and  $1.8$  g/cm<sup>3</sup> for the organic and sulfuric acid-water, respectively (65), and  $R = 8.3 \times 10^7$  dyn-cm/K-mol,  $T = 300$  K, and  $P^0_{\text{ORG}} = P^0_{\text{H}_2\text{SO}_4}$  we calculate  $P_{\text{ORG}}/P_{\text{H}_2\text{SO}_4} = \sim 10^{10}$  for 1 nm particles, which is the approximate size of critical nuclei. The Kelvin effect therefore favors nucleation of sulfuric acid-water over organics.

Once nucleation has occurred, particles grow by condensation of organic compounds. The rate at which a compound adds to a particle depends on the difference between rates of compound condensation and evaporation, which in turn depends on the difference between the partial pressure and equilibrium vapor pressure of the compound. Because of the Kelvin effect, the equilibrium vapor pressure of a compound increases with decreasing particle size. The magnitude of this effect is significant for particles smaller than 100 nm in diameter. Therefore, it is expected that diesel nanoparticles will initially grow by addition of lower volatility compounds, with growth by condensation of higher volatility components increasing with particle size. Our observation that the volatility of particle components decreases with decreasing particle size is consistent with this process of particle growth.

## **6. CONCLUSIONS**

The Nano-DMA/TDPBMS technique used here yields important information on the chemical composition of diesel nanoparticles in near-real time. In addition to detecting low concentrations of sulfuric acid in particles as small as ~40 nm MMD, it also provides useful data on the identities and vapor pressures of the organic components, which make up the bulk of the particle mass, for sizes down to ~25 nm MMD. The results obtained thus far are consistent with a mechanism of diesel nanoparticle formation involving homogeneous binary nucleation of sulfuric acid and water followed by particle growth from condensation of organic species onto the sulfuric acid-water core. Future studies need to focus on measuring the composition of smaller particles than were measured here in order to gain a more detailed description of the nucleation and growth processes. The Nano-DMA/TDPBMS approach will also be valuable for investigating the effects of engine operating conditions, fuel and lubricating oil (especially sulfur content), dilution conditions, temperature, and relative humidity on nanoparticle formation from various engines. Because of the near-real time nature of the technique, such studies can be performed much more rapidly and comprehensively than is possible with traditional instrumentation.

## 7. FUTURE PLANS

The TDPBMS is running again after having been down for a few months after the UMN study. A new programmable power supply for the particle vaporizer has been purchased and Labview software is being written so as to provide better-controlled, more reproducible temperature ramps for fast-TPTD analysis. In the near future, experiments will be performed on mixed PAH/alkane particles to determine the extent to which PAH signal can be enhanced by operating the vaporizer at high temperatures and the ionizer at 200 eV.

UMN analysis of nanoparticle size data obtained using the unipolar charger has provided us with a possible means to further optimize the performance of this charger and therefore enhance TDPBMS signal/noise for nanoparticle analysis. We now think that by using the spreadsheet calculation procedure developed previously, we can determine the residence time in the charger that will give the highest concentration of singly charged particles while minimizing the fractions of multiply-charged particles. The residence time will be controlled by changing the flowrate into the charger. At UMN further thought is being given to possible ways of evaluating and possibly improving the performance of the electrostatic lens and determining the transport efficiencies of diesel nanoparticles into the TDPBMS. One possibility being considered is to collect nanoparticles for microscopic analysis of the beam deposit spot size and particle sample heterogeneity.

UCR and UMN have begun planning discussions for the Phase 2 Caterpillar study in Fall 2000. Based on his experiences at the recent Cummins study, Professor Kittelson strongly recommended that instead of taking the TDPBMS to the Caterpillar facility, we return to UMN and sample from their recently-installed, modern Caterpillar engine. This approach is preferable for a number of reasons: (1) we have already performed a successful study at UMN and are thoroughly familiar with the facilities and personnel, (2) the UMNCDR facility provides a more flexible research environment, which as we learned from the UMN study, can be critical for successfully operating the technically sophisticated, state-of-the-art, TDPBMS, and (3) we would not be limited to the same two-week time frame as at the Caterpillar facility. The overall chances of success would therefore be greatly enhanced. The CRC and ARB are in favor of this approach, with the primary concern being that the work will be performed within the original budget and not change in scope. Professor Kittelson has indicated that sufficient funds will be provided by Caterpillar to run the engine using graduate students working in the CDR. The project funds for the Cummins study in 2001 will not be affected by changing the location of the Caterpillar study to UMN. The current plan is to perform approximately two weeks of experiments at UMN beginning in early October, 2000. The TDPBMS will be shipped from UCR in late September, and reassembled and tested approximately one week in advance of the study. The experiments to be performed will be similar to those carried out during Phase 1. While these experiments are going on some additional measurements will be made, including tandem nano-differential mobility measurements by the McMurry group to investigate the volatility and hygroscopic properties of the nanoparticles. These data can be used to gain additional information on the heterogeneity of the nanoparticle aerosol, the amount of sulfuric acid present, and the molecular weights of organic components. Professor Kittelson's group will be collecting nano-MOUDI samples for analysis of elemental carbon, organic carbon, sulfate, and metals.

## 8. REFERENCES

- (1) Pope, C. A.; Thun, M. J.; Namboodiri, M. M.; Dockery, D. W.; Evans, J. S.; Speizer, F. E.; Heath, C. W. *Am. J. Respir. Crit. Care Med.* **1995**, *151*, 669-674.
- (2) Seaton, A.; MacNee, W.; Donaldson, K.; Godden, D. *Lancet* **1995**, *345*, 176-179.
- (3) Kittelson, D. B. *J. Aerosol Sci.* **1998**, *29*, 575-588.
- (4) Ferin, J.; Oberdorster, G.; Penny, D. P. *Am. J. Respir. Cell Mol. Biol.* **1992**, *6*, 535-542.
- (5) Donaldson, K.; Beswick, P. H.; Gilmour, P. S. *Toxicol. Lett.* **1996**, *88*, 293-298.
- (6) Oberdorster, G. *Inhal. Toxicol.* **1996**, *8*, 73-89.
- (7) Donaldson, K.; Li, X. Y.; MacNee, W. *J. Aerosol Sci.* **1998**, *29*, 553-560.
- (8) Simoneit, B. R. T. *Atmos. Environ.* **1984**, *18*, 51-67.
- (9) Simoneit, B. R. T. *Int. J. Environ. Anal. Chem.* **1985**, *22*, 203-233.
- (10) Rogge, W. F.; Hildemann, L. M.; Mazurek, M. A.; Cass, G. R.; Simoneit, B. R. T. *Environ. Sci. Technol.* **1993**, *27*, 636-651.
- (11) Schauer, J. J.; Kleeman, M. J.; Cass, G. R.; Simoneit, B. R. T. *Environ. Sci. Technol.* **1999**, *33*, 1578-1587.
- (12) Shi, J. P.; Mark, D.; Harrison, R. M. *Environ. Sci. Technol.* **2000**, *34*, 748-755.
- (13) Kleeman, M. J.; Schauer, J. J.; Cass, G. R. *Environ. Sci. Technol.* **2000**, *34*, 1132-1142.
- (14) Shi, J. P.; Harrison, R. M. *Environ. Sci. Technol.* **1999**, *33*, 3730-3736.
- (15) Marple, V. A.; Rubow, K. L.; Behm, S. M. *Aerosol Sci. Technol.* **1991**, *14*, 434-446.
- (16) McMurry, P. H. *Atmos. Environ.* **2000**, *34*, 1959-1999.
- (17) Chen, D. R.; Pui, D. Y. H.; Hummes, D.; Fissan, H.; Quant, F. R.; Sem, G. J. *J. Aerosol Sci.* **1998**, *29*, 497-509.
- (18) Tobias, H. J.; Ziemann, P. J. *Anal. Chem.* **1999**, *71*, 3428-3435.
- (19) Tobias, H. J.; Kooiman, P. M.; Docherty, K. S.; Ziemann, P. J. *Aerosol Sci. Technol.* in press.
- (20) Tobias, H. J.; Ziemann, P. J. *Environ. Sci. Technol.* **2000**, *34*, 2105-2115.
- (21) Tobias, H. J.; Docherty, K. S.; Beving, D. E.; Ziemann, P. J. *Environ. Sci. Technol.* **2000**, *34*, 2116-2125.
- (22) Khalek, I. A.; Kittelson, D. B. *SAE Tech. Pap. Ser.* **1999**, 1999-01-1142.
- (23) Khalek, I. A.; Kittelson, D. B.; Brear, F. *SAE Tech. Pap. Ser.* **2000**, No. 2000-01-0515.
- (24) Chen, D. R.; Pui, D. Y. H. *Journal of Nanoparticle Research* **1999**, *1*, 115-126.
- (25) Liu, B. Y. H.; Pui, D. Y. H. *J. Colloid Interface Sci.* **1974**, *49*, 305-311.
- (26) Liu, B. Y. H.; Pui, D. Y. H. *J. Colloid Interface Sci.* **1974**, *47*, 155-171.
- (27) Knutson, E. O. *J. Aerosol Sci.* **1975**, *6*, 443-451.
- (28) Wang, S. C.; Flagan, R. C. *Aerosol Sci. Technol.* **1990**, *13*, 230-240.
- (29) Fuchs, N. A. *Geophys. Pura Appl.* **1963**, *56*, 185-193.
- (30) Pui, D. Y. H.; Fruin, S.; McMurry, P. H. *Aerosol Sci. Technol.* **1988**, *8*, 173-187.
- (31) Liu, P.; Ziemann, P. J.; Kittelson, D. B.; McMurry, P. H. *Aerosol Sci. Technol.* **1995**, *22*, 293-313.
- (32) Liu, P.; Ziemann, P. J.; Kittelson, D. B.; McMurry, P. H. *Aerosol Sci. Technol.* **1995**, *22*, 314-324.
- (33) Kinney, P. D.; Pui, D. Y. H.; Mulholland, G. W.; Bryner, N. P. *J. Res. Natl. Inst. Stand. Technol.* **1991**, *96*, 147-176.
- (34) Black, F.; High, L. *SAE Tech. Pap. Ser.* **1979**, No. 790422.
- (35) Cartellieri, W.; Tritthart, P. *SAE Tech. Pap. Ser.* **1984**, No. 840418.

- (36) Siegl, W. O.; Hammerle, R. H.; Herrmann, H. M.; Wenclawiak, B. W.; Luers-Jongen, B. *Atmos. Environ.* **1999**, *33*, 797-805.
- (37) Petrov, A. A. *Petroleum Hydrocarbons*; Springer-Verlag: New York, 1984.
- (38) Tissot, B. P.; Welte, D. H. *Petroleum Formation and Occurance*; Springer-Verlag: New York, 1984.
- (39) Kissin, Y. V. *Fuel* **1990**, *10*, 1283-1291.
- (40) Hildemann, L. M.; Markowski, G. R.; Cass, G. R. *Environ. Sci. Technol.* **1991**, *25*, 744-759.
- (41) Hood, A. *Mass Spectra of Organic Ions*; Academic Press: New York, 1963.
- (42) McLafferty, F. W.; Turecek, F. *Interpretation of Mass Spectra*, 4th ed.; University Science Books: Sausalito, CA, 1993.
- (43) Simoneit, B. R. T., personal communication.
- (44) Simoneit, B. R. T. In *Chemistry and Analysis of Hydrocarbons in the Environment*; Albaiges, J., Frei, R. W., Merian, E., Eds.; Gordon and Breach Science Publishers: New York, 1983; Vol. 5, pp 147-163.
- (45) Philp, R. P. *Mass Spectrom. Rev.* **1985**, *4*, 1-54.
- (46) Simoneit, B. R. T.; Cardoso, J. N.; Robinson, N. *Chemosphere* **1990**, *21*, 1285-1301.
- (47) Schauer, J. J.; Rogge, W. F.; Hildemann, L. M.; Mazurek, M. A.; Cass, G. R.; Simoneit, B. R. T. *Atmos. Environ.* **1996**, *30*, 3837-3855.
- (48) Lowenthal, D. H.; Zielinska, B.; Chow, J. C.; Watson, J. G.; Gautum, M.; Ferguson, D. H.; Neuroth, G. R.; Stevens, K. D. *Atmos. Environ.* **1994**, *28*, 731-743.
- (49) Tancell, P. J.; Rhead, M. M.; Pemberton, R. D.; Braven, J. *Environ. Sci. Technol.* **1995**, *29*, 2871-2876.
- (50) Marr, L. C.; Kirchstetter, T. W.; Harley, R. A.; Miguel, A. H.; Hering, S. V.; Hammond, S. K. *Environ. Sci. Technol.* **1999**, *33*, 3091-3099.
- (51) Gross, D. S.; Galli, M. E.; Silva, P. J.; Wood, S. H.; Lui, D.-Y.; Prather, K. A. *Aerosol Sci. Technol.* **2000**, *32*, 152-163.
- (52) Finnlayson-Pitts, B. J.; Pitts, J. *Chemistry of the Upper and Lower Atmosphere*; Academic Press, 1999.
- (53) Schwarzenbach, R. P.; Gschwend, P. M.; Imboden, D. M. *Environmental Organic Chemistry*; Wiley & Sons: New York, 1993.
- (54) Pankow, J. F. *Environ. Sci. Technol.* **1994**, *28*, 363-365.
- (55) Piacente, V.; Fontana, D.; Scardala, P. *J. Chem. Eng. Data* **1994**, *39*, 231-237.
- (56) Richardson, C. B.; Hightower, R. L.; Pigg, A. L. *App. Optics* **1986**, *25*, 1226-1229.
- (57) Crable, G. F.; Coggeshall, N. D. *Anal. Chem.* **1958**, *30*, 310-313.
- (58) Lampe, F. W.; Franklin, J. L.; Field, F. H. *J. Am. Chem. Soc.* **1957**, *79*, 6129-6132.
- (59) Orient, O. J.; Srivastava, S. K. *J. Chem. Phys.* **1984**, *80*, 140-143.
- (60) Smith, O. I.; Stevenson, J. S. *J. Chem. Phys.* **1981**, *74*, 6777-6783.
- (61) Morrison, R. T.; Boyd, R. N. *Organic Chemistry*, 3rd ed.; Allyn and Bacon: Boston, 1973.
- (62) Adamson, A. W. *Physical Chemistry of Surfaces*, 4th ed.; John Wiley & Sons: New York, 1982.
- (63) Weber, R. J.; Marti, J. J.; McMurry, P. H.; Eisele, F. L.; Tanner, D. J.; Jefferson, A. *Chem. Eng. Comm.* **1996**, *151*, 53-64.
- (64) Weber, R. J.; McMurry, P. H.; Mauldin, L.; Tanner, D. J.; Eisele, F. L.; Brechtel, F. J.; Kreidenweis, S. M.; Kok, G. L.; Schillawski, R. D.; Baumgardner, D. *J. Geophys. Res.* **1998**, *103*, 16385-16396.

- (65) Seinfeld, J. H.; Pandis, S. N. *Atmospheric Chemistry and Physics*; John Wiley & Sons, Inc.: New York, 1998.

## 9. FIGURES AND TABLES

Figure 1. Schematic of the apparatus used for diesel exhaust particle generation (medium-duty diesel engine), dilution (VRTDS), charging (unipolar and bipolar chargers), size selection (Nano-DMA), and chemical analysis (TDPBMS). Solid circles refer to valves, and arrowheads indicate the direction of aerosol flow. The apparatus was used in various configurations as follows, where letters listed for each mode refer to valves that are open, while the remaining valves are closed: total-mode = A and I; large nano-mode = B, C, and G; small nano-mode = B, D, and G; SMPS = A and H; Nano-SMPS = B and E; Tandem DMA = B, C or D, and F.

Figure 2. Number (solid symbols) and mass (open symbols) distributions for diesel exhaust particles in the (A) total-mode at 15% (circles) and 50% (triangles) engine load, (B) large nano-mode at 15% engine load, and (C) small nano-mode at 15% engine load.

Figure 3. Fast-TPTD mass spectra of diesel engine particles acquired at the signal maximum during desorption. Analyzed particles include those in the large nano-mode at 15% engine load with MMD of (A) 34 nm and (B) 29 nm, and (C) total-mode at 50% engine load.

Figure 4. Fast-TPTD mass spectra acquired at the signal maximum during desorption of aerosol standards of (A) diesel fuel, (B) lubricating oil, and (C) sulfuric acid. Peak desorption temperatures are given in parentheses.

Figure 5. Columns A-D excluding DIII are fast-TPTD  $m/z$  69 mass thermograms of diesel exhaust particles acquired using the five-mass SIM method. Analyses were conducted at (column A) 15%, (column B) 25%, (column C) 40%, and (DI, DII) 50% engine loads on (row I) total, (row II) large nano, and (row III excluding DIII) small nano-mode particles. (DIII) Diesel exhaust gas background measured at 50% engine load. The sample MMD is given in parentheses.

Figure 6. Correlation between n-alkane (hexadecane, eicosane, tetracosane, octacosane, and dotriacontane) vapor pressures at 25°C (solid circles, left hand ordinate) and carbon number (open circles, right hand ordinate), and desorption temperatures measured by fast-TPTD.

Figure 7. Fast-TPTD mass thermograms of aerosol standards of (A) fuel, (B) lubricating oil, (C) sulfuric acid, and (D) sulfuric acid/ammonium sulfate.

Figure 8. Columns A-D excluding DIII are fast-TPTD  $m/z$  98 mass thermograms of diesel exhaust particles acquired using the five-mass SIM method. Analyses were conducted at (column A) 15%, (column B) 25%, (column C) 40%, and (DI, DII) 50% engine loads on (row I) total, (row II) large nano, and (row III excluding DIII) small nano-mode particles. (DIII) Diesel exhaust gas background measured at 50% engine load. The sample MMD is given in parentheses.

Figure 9. Columns A-D excluding DIII are fast-TPTD  $m/z$  85 mass thermograms of diesel exhaust particles acquired using the five-mass SIM method. Analyses were conducted at (column A) 15%, (column B) 25%, (column C) 40%, and (DI, DII) 50% engine loads on (row I) total, (row II) large nano, and (row III excluding DIII) small nano-mode particles. (DIII) Diesel exhaust gas background measured at 50% engine load. The sample MMD is given in parentheses.

Figure 10. Columns A-D excluding DIII are fast-TPTD  $m/z$  95 mass thermograms of diesel exhaust particles acquired using the five-mass SIM method. Analyses were conducted at (column A) 15%, (column B) 25%, (column C) 40%, and (DI, DII) 50% engine loads on (row I) total, (row II) large nano, and (row III excluding DIII) small nano-mode particles. (DIII) Diesel exhaust gas background measured at 50% engine load. The sample MMD is given in parentheses.

Figure 11. Columns A-D excluding DIII are fast-TPTD  $m/z$  81 mass thermograms of diesel exhaust particles acquired using the five-mass SIM method. Analyses were conducted at (column A) 15%, (column B) 25%, (column C) 40%, and (DI, DII) 50% engine loads on (row I) total, (row II) large nano, and (row III excluding DIII) small nano-mode particles. (DIII) Diesel exhaust gas background measured at 50% engine load. The sample MMD is given in parentheses.

**Table 1.** Matrix of Diesel Exhaust Particle Mode Analyses

Engine Load (%)	Complete Mass Spectrum			Five-mass SIM		
	mode	mass mean diam. (nm)	# peak diam. (nm)	mode	mass mean diam. (nm)	# peak diam. (nm)
15	large nano	34 and 29	29	small nano	26	24
				large nano	40	24
				total	N/A	21
25				small nano	31	24
				large nano	38	23
				total	N/A	17
40				small nano	30	24
				large nano	41	N/A
				total	N/A	N/A
50	total	N/A	29	small nano	27	N/A
				large nano	58	15
				total	N/A	17



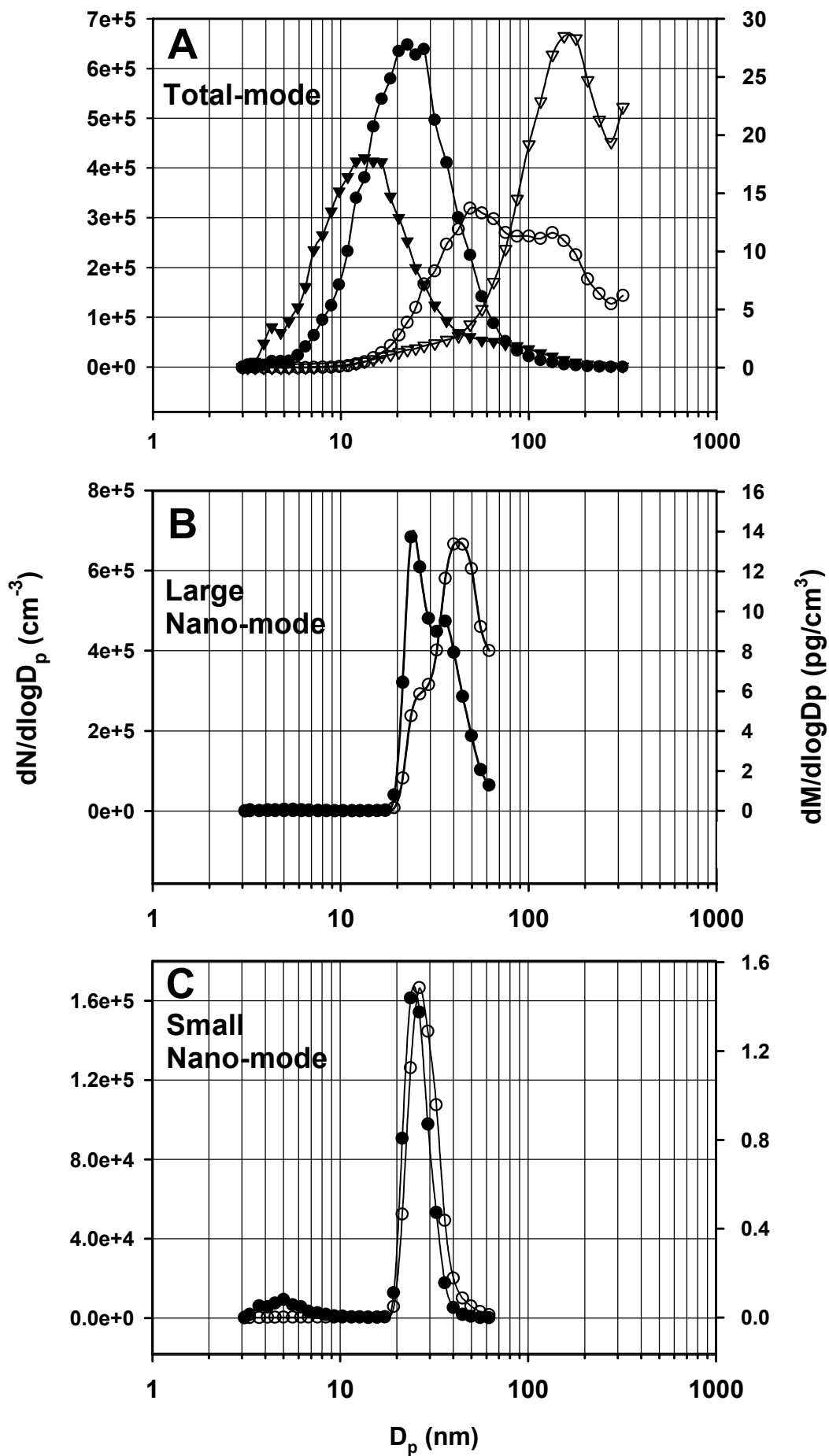
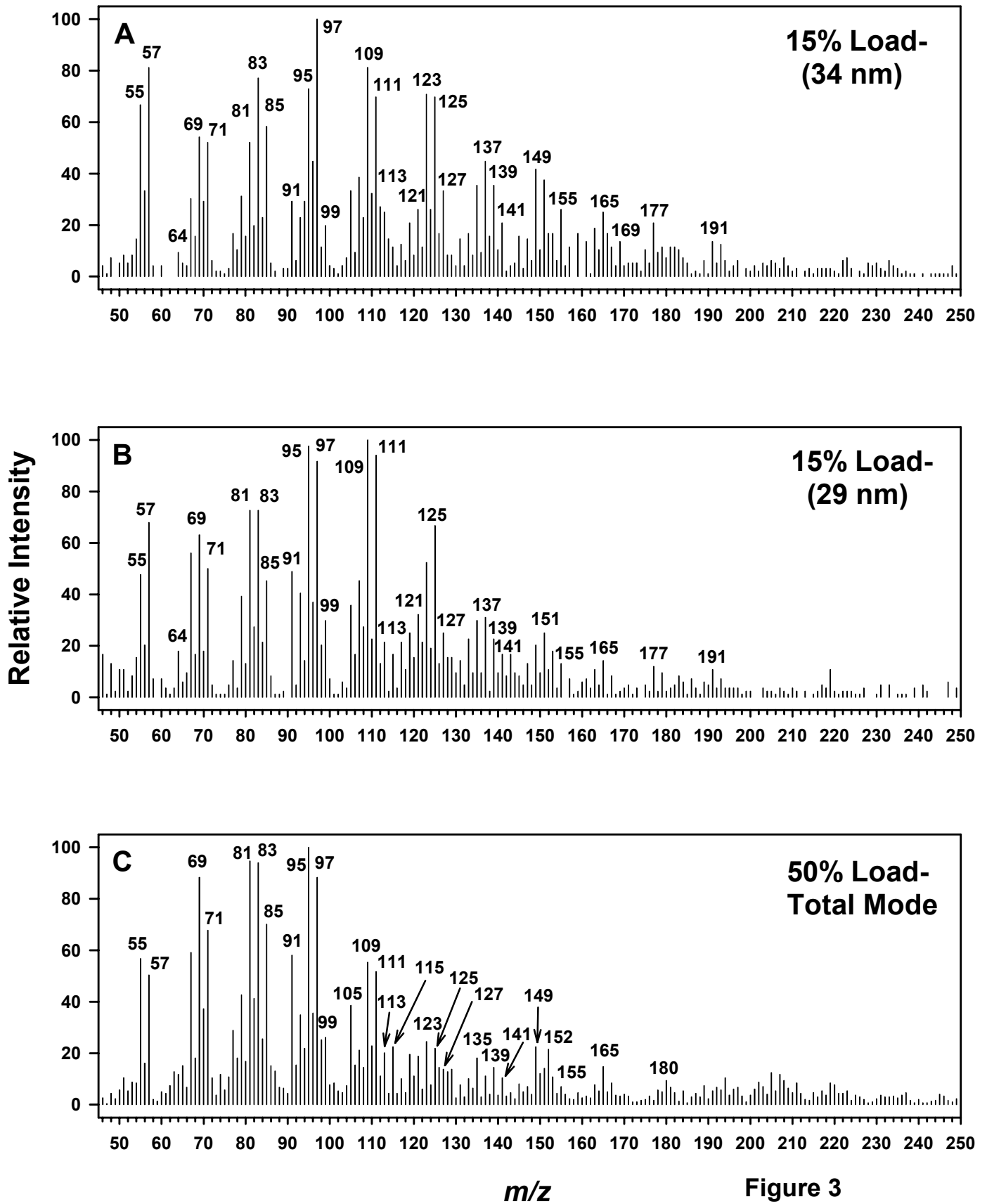
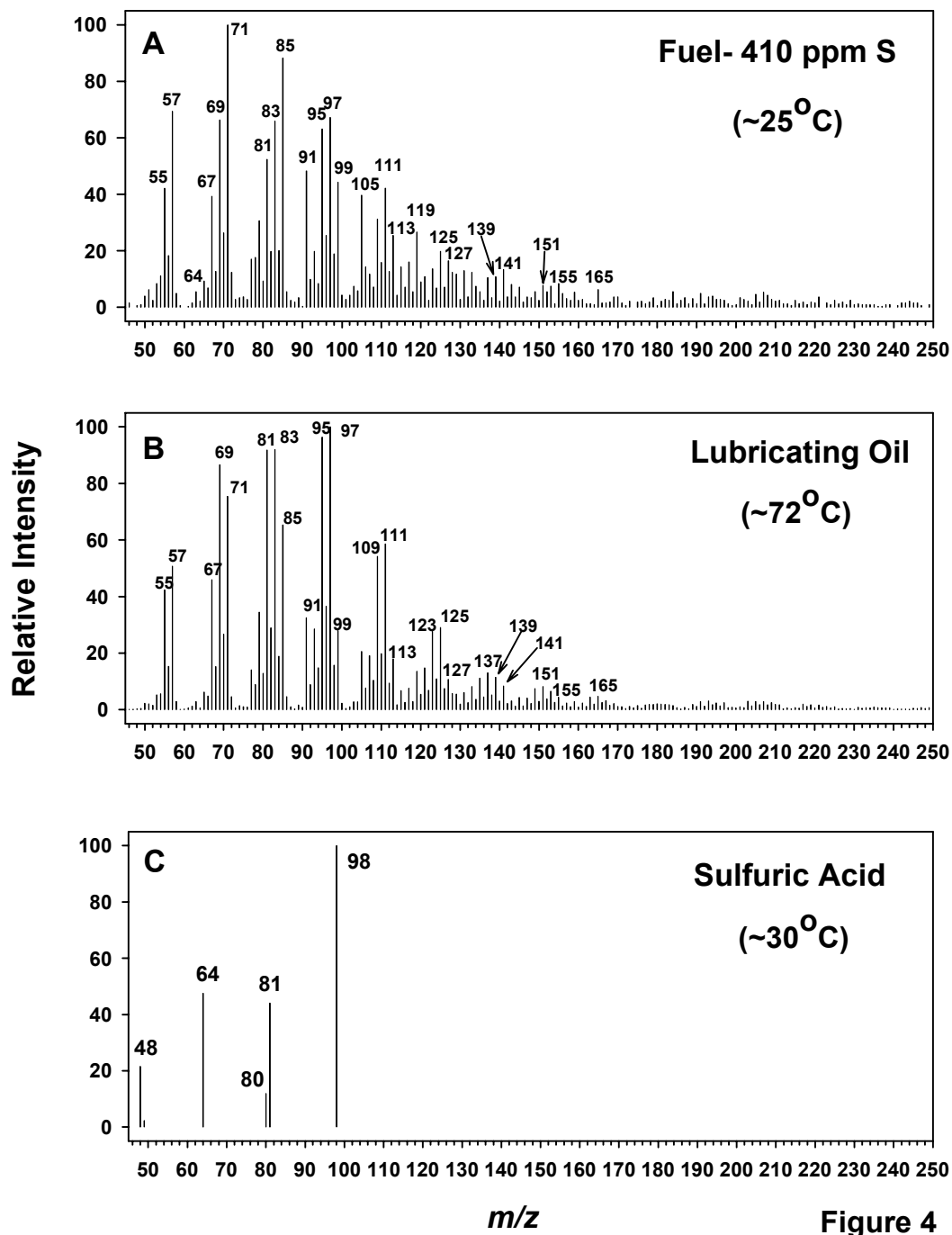


Figure 2





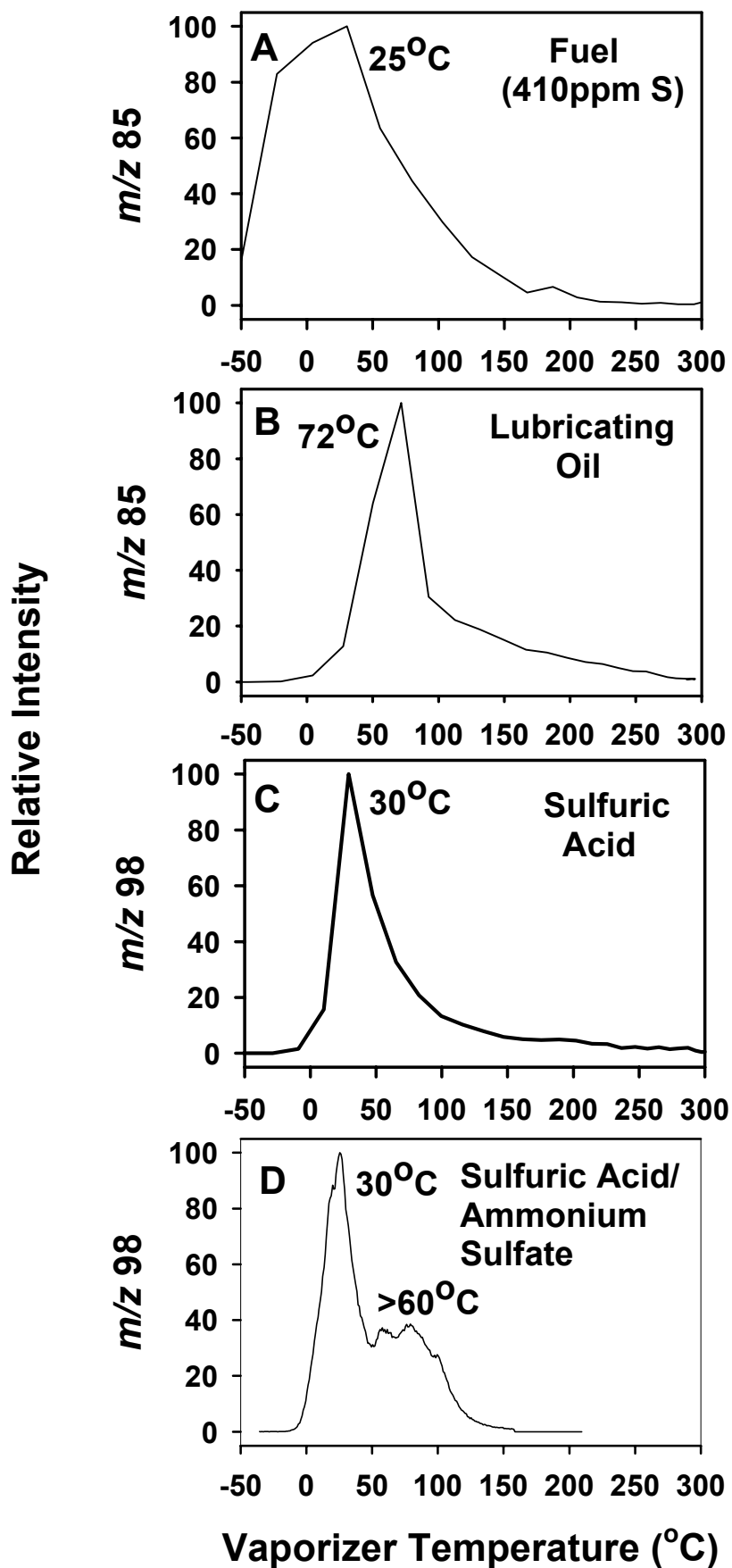


Figure 7

